





# Airborne Bioaerosol Observations Imply a Strong Terrestrial Source in the Summertime Arctic

Anne E. Perring<sup>1,2</sup> , Braden Mediavilla<sup>1,3</sup> , G. Dewey Wilbanks<sup>1,4</sup>, James H. Churnside<sup>5</sup>, Richard Marchbanks<sup>2,5</sup>, Kara D. Lamb<sup>2,5,6</sup> , and Ru-Shan Gao<sup>5</sup> 

<sup>1</sup>Department of Chemistry, Colgate University, Hamilton, NY, USA, <sup>2</sup>Cooperative Institute for Research in Environmental Sciences, University of Colorado Boulder, Boulder, CO, USA, <sup>3</sup>Now at Department of Chemistry, Johns Hopkins University, Baltimore, MD, USA, <sup>4</sup>Now at Weill-Cornell Medicine, New York, NY, USA, <sup>5</sup>Earth Systems Research Laboratory, National Oceanic and Atmospheric Administration, Boulder, CO, USA, <sup>6</sup>Now at Department of Earth and Environmental Engineering, Columbia University, New York, NY, USA

### Key Points:

- High loadings of fluorescent biological aerosol observed over the summertime Arctic, associated with remarkably warm air temperatures
- Back trajectories indicate a terrestrial source for these particles with estimated emission rates comparable to those for the continental US
- No evidence of biological aerosol emission from the surface ocean

### Supporting Information:

Supporting Information may be found in the online version of this article.

### Correspondence to:

A. E. Perring,  
[aperring@colgate.edu](mailto:aperring@colgate.edu)

### Citation:

Perring, A. E., Mediavilla, B., Wilbanks, G. D., Churnside, J. H., Marchbanks, R., Lamb, K. D., & Gao, R.-S. (2023). Airborne bioaerosol observations imply a strong terrestrial source in the summertime Arctic. *Journal of Geophysical Research: Atmospheres*, 128, e2023JD039165. <https://doi.org/10.1029/2023JD039165>

Received 27 APR 2023

Accepted 26 JUL 2023

Corrected 23 SEP 2023

This article was corrected on 23 SEP 2023. See the end of the full text for details.

### Author Contributions:

**Conceptualization:** James H. Churnside

**Data curation:** James H. Churnside

**Formal analysis:** Braden Mediavilla, G. Dewey Wilbanks, James H. Churnside

**Funding acquisition:** James H. Churnside

**Investigation:** James H. Churnside

**Methodology:** James H. Churnside

**Project Administration:** James H. Churnside

**Resources:** James H. Churnside

**Writing – review & editing:** Braden Mediavilla, G. Dewey Wilbanks, James H. Churnside

**Writing – review & editing:** Braden Mediavilla, G. Dewey Wilbanks, James H. Churnside

**Writing – review & editing:** Braden Mediavilla, G. Dewey Wilbanks, James H. Churnside

**Writing – review & editing:** Braden Mediavilla, G. Dewey Wilbanks, James H. Churnside

**Writing – review & editing:** Braden Mediavilla, G. Dewey Wilbanks, James H. Churnside

**Writing – review & editing:** Braden Mediavilla, G. Dewey Wilbanks, James H. Churnside

**Writing – review & editing:** Braden Mediavilla, G. Dewey Wilbanks, James H. Churnside

**Writing – review & editing:** Braden Mediavilla, G. Dewey Wilbanks, James H. Churnside

**Writing – review & editing:** Braden Mediavilla, G. Dewey Wilbanks, James H. Churnside

**Writing – review & editing:** Braden Mediavilla, G. Dewey Wilbanks, James H. Churnside

**Writing – review & editing:** Braden Mediavilla, G. Dewey Wilbanks, James H. Churnside

**Writing – review & editing:** Braden Mediavilla, G. Dewey Wilbanks, James H. Churnside

**Writing – review & editing:** Braden Mediavilla, G. Dewey Wilbanks, James H. Churnside

**Writing – review & editing:** Braden Mediavilla, G. Dewey Wilbanks, James H. Churnside

**Writing – review & editing:** Braden Mediavilla, G. Dewey Wilbanks, James H. Churnside

**Writing – review & editing:** Braden Mediavilla, G. Dewey Wilbanks, James H. Churnside

**Abstract** Primary biological aerosol (PBA) is a component of coarse mode aerosol which may affect climate and health. The possible climate impacts arise from interactions between PBA and water vapor, especially since some PBA nucleate ice at warm temperatures. The health impacts span from seasonal allergies to transmission of pathogens. Despite their potential importance, the emissions, transport, and atmospheric distribution of PBA are poorly understood, especially at high latitudes where cloud effects could be pronounced. Here we report summertime measurements of fluorescent aerosol (a proxy for PBA) over the Bering and Chukchi Seas using a Wide-Band Integrated Bioaerosol Sensor aboard a Twin Otter, alongside a lidar which detected water column productivity. Most observations occurred at 300 m over the ocean with periodic excursions to 60 and 900 m. Loadings were always low in the marine boundary layer, despite the presence of subsurface plankton layers and in contrast to other recent reports, likely indicating low oceanic emissions during our study. Large variability was observed in PBA aloft, with higher concentrations approaching those observed over the Continental US. Back trajectory analysis showed that high loadings were associated with recent transit through the continental boundary layer and we estimate PBA emissions from the Arctic tundra of up to 300 m<sup>-2</sup> s<sup>-1</sup> at the warmest observed temperatures. On days with strong transport from land (~50% of our flights), PBA accounts for 12% of supermicron number and 64% of supermicron volume, indicating potentially significant effects on the albedo, glaciation and lifetime of Arctic clouds.

**Plain Language Summary** Cloud cover affects Earth's temperature because clouds reflect sunlight back to space. Biological particles can cause warm clouds to freeze sooner than most other materials. This makes the clouds go away faster and reflect less sunlight. In the warming Arctic, ice, and snow (which also reflect sunlight) are melting, exposing water. Water absorbs sunlight, which makes cloud cover even more important. At the same time, Arctic ecosystems are changing, and might emit more biological particles in response. We measured biological particles over the Arctic Ocean. We found more than we were expecting and we think most of them came from land. This could change how Arctic clouds behave in important ways. As the Arctic continues to warm there might be even more of these particles in the future.

## 1. Introduction

Primary biological aerosol (PBA), also often termed bioaerosol, consists primarily of airborne viruses, bacteria, spores, and pollen and their component parts. PBA is an area of growing interest to the atmospheric community as it has been shown to be a considerable fraction of aerosol mass in certain environments (Huffman et al., 2013; Perring et al., 2015; Pöschl et al., 2010) which may have important implications for cloud formation, cloud glaciation and precipitation (DeMott & Prenni, 2010; Fröhlich-Nowoisky et al., 2016). The cloud impacts of PBA arise, in part, from the fact that some PBA are capable of nucleating ice at remarkably warm temperatures, within a few degrees of 0°C. Biological particles have been observed in precipitation from around the globe (Christner et al., 2008) and in ice-cloud residuals (Creamean et al., 2013; Pratt et al., 2009) and it is thought that most warm temperature (>−15°C) ice nuclei (IN) are biological in origin (Murray et al., 2012). In addition, PBA may also affect cloud behavior by acting as giant CCN (Möhler et al., 2007). The precise relationship between PBA concentrations and the lifetime, albedo, and precipitation characteristics of clouds remains uncertain and

increased knowledge of the sources, seasonality and characteristics of PBA emissions in different environments is necessary.

The Arctic is warming more quickly in response to climate change than lower-latitude locations, a phenomenon known as Arctic amplification (reviewed in Serreze & Barry, 2011). Some of the primary mechanisms posited to cause this amplification include a surface albedo feedback resulting from reduced snow and ice cover (e.g., Dai, 2021), an albedo feedback resulting from changes in cloud cover (Wang & Key, 2005) and increasing poleward heat transport in response to changing circulation patterns (Gong et al., 2017; Hwang et al., 2011) though there is debate about the exact operation of each mechanism and their relative importance. There are also many other potential contributors to Arctic amplification and it is a very active area of research. See, for example, a recent review by You et al. (2021) and references therein. In terms of the topic of the present work, PBA may contribute to Arctic amplification via their cloud interactions, especially because declining sea ice is expected to make the region increasingly sensitive to the behavior of clouds, which can reflect incoming sunlight back to space before it is absorbed by the dark ocean surface (H. Morrison et al., 2012; Prenni et al., 2007; Verlinde et al., 2007). Finally, it is likely that sources of PBA to the Arctic may change in response to climate-driven ecological shifts. Thus, the Arctic is a very interesting and important location in which to characterize PBA.

Remarkably high warm-temperature IN concentrations have recently been observed in a number of locations in the Arctic, potentially indicating the presence of unknown PBA emissions in the region. Wex et al. (2019) report concentrations from a land-based observatory and hypothesize that their warm temperature IN arise from forested ecosystems in Scandinavia. They note, however, that their observations do not necessarily indicate that these biological particles are efficiently transported over the open ocean nor that they are exported to the mixed layer where the effects on clouds would be most pronounced. Porter et al. (2022) report very high IN concentrations at the North Pole, which they attribute to a wind-driven marine biological source transported from the Russian coastline. Others (Bigg & Leck, 2001; Creamean et al., 2019; Hartmann et al., 2020) have attributed warm-temperature IN observed over the Arctic Ocean to an oceanic biological source emitted either from the open ocean or broken leads. Hartmann et al. (2021) find a lack of clear terrestrial influence and thus infer a predominant oceanic source for IN in the Arctic, yet also report that the known oceanic source is far too small to explain the observed atmospheric IN. Thus, it appears likely that the region is affected both by local oceanic emissions and long-range transport of biological material from coastal or terrestrial regions and it is interesting to consider the variable seasonality of these sources and how they might change in response to a warming environment. Most of these measurements have been collected at the surface which makes it difficult to infer concentrations available at the level of cloud formation. Porter et al. (2022) report measurements from balloon soundings, which show distinctly different IN concentrations in the surface mixed layer over the ocean as compared to the cloud mixed layer above, further bolstering the need for more widespread observations of IN or related quantities above the surface layer over the Arctic Ocean.

Here we report measurements of fluorescent aerosol, which we use as a proxy for PBA, from a NOAA Twin Otter which flew out of Utqiaġvik in the summer of 2017. Although PBA measurements are one step removed from direct observations of IN concentrations, they can be used to estimate IN via previously observed relationships (Tobo et al., 2013) and they may lend themselves more to source attribution than do direct observations of IN. Additionally, because the instrument used records single-particle fluorescence in real-time, it is relatively easy to sample a large geographic area and to probe multiple altitudes, as the required integration times are relatively short. Here we measured within the marine boundary and at two higher altitudes so we are able to comment on local oceanic emission as well as more regional sources.

## 2. Materials and Methods

Measurements were made during the summer of 2017 aboard a NOAA Twin Otter aircraft. The aircraft was equipped with a Wide-Band Integrated Bioaerosol Sensor (WIBS-4A) (Droplet Measurement Technologies, Longmont, CO) to detect single particle aerosol optical size and fluorescence, a lidar to detect sub-surface plankton concentrations and an aircraft-integrated meteorological measurement system (Matthews & Goldberger, 2020), mounted on the outside of the aircraft, which provided meteorological data. Descriptions of the WIBS and the lidar, details regarding the inlet and sampling strategy for in situ aerosol and data sets used to generate HYSPLIT back trajectories are given below.

### 2.1. The Wideband Integrated Bioaerosol Sensor

The WIBS-4A is a commercially-available (Droplet Measurement Technologies, Boulder, CO) single-particle fluorescence sensor that has been described in detail previously (Gabey et al., 2010; Healy et al., 2012; Kaye et al., 2005; Perring et al., 2015). Briefly, ambient air is drawn into the detection cell and directed through a 635 nm laser. Aerosol particles present in the airstream produce side-scattered light, which is imaged onto a photomultiplier tube and used to determine the optical size of individual particles. This signal also triggers the sequential firing of two Xenon lamps filtered to emit at 280 and 370 nm. Autofluorescence arising from the excitation pulses is imaged onto two PMTs filtered to detect light in wavebands from 310 to 400 nm (often termed the FL1 detector) and 420–650 nm (often termed the FL2 detector). Each particle therefore results in three possible fluorescence signals: fluorescence detected between 310 and 400 nm following 280 nm excitation (denoted here as Channel A), fluorescence detected between 420 and 650 nm following 280 nm excitation (denoted here as Channel B) and fluorescence detected between 420 and 650 nm following 370 nm excitation (denoted here as Channel C). The 370 nm flash saturates the FL1 detector so there is no signal associated with 310–400 nm emission following 370 nm excitation.

The excitation wavelengths and detection bands correspond to the excitation and emission of various bio-fluorophores such as tryptophan, NADH, and flavins, although there are also non-biological fluorescent compounds with overlapping excitation/emission spectra. Potential non-biological interferences have been explored in several laboratory studies (Pöhlker et al., 2012; Savage et al., 2017) and include certain kinds of dust and humic material as well as both diesel and flame-generated black carbon aerosol. The present work uses the analysis framework introduced by Perring et al. (2015) whereby fluorescent particles are identified by the combination of fluorescence signals which they exhibit. A particle with signal only in channel A (280 nm excitation, 310–400 nm emission) and not in either of the other channels, for example, is denoted as type A. A particle exhibiting signal in channels A and B (280 nm excitation, 310–400 nm emission) and not in C is referred to as type AB, while a particle which exhibits signal in all three channels is termed type ABC. Papers examining laboratory-generated PBAP using this framework (Hernandez et al., 2016; Savage et al., 2017) find that bacteria typically manifest as type A at sizes near 1  $\mu\text{m}$ , spores typically manifest as a combination of types A, AB, and ABC at sizes between 2 and 5  $\mu\text{m}$  and pollen manifests as a combination of types B, BC, and ABC at a wide range of sizes dependent on the extent to which the pollen grain has fractionated into smaller particles. Savage et al. (2017) also investigated the WIBS response to potentially fluorescent non-biological materials like soot (primarily types A or B), dust (types A, B, and AB), humic material (types B and BC) and brown carbon (different types for different samples). As discussed below, non-biological materials are often more weakly fluorescent than biological materials and thus their impact can be partially mitigated through data processing choices.

In addition to any particle-induced fluorescence, there is some background signal in each channel resulting from flash lamp light that leaks through the filters to the detectors as well as any stray fluorescence within the detection cell (from either gas-phase species or compounds adhered to the walls of the detection cell). This background signal is monitored by periodically running the WIBS in “Forced Trigger” mode whereby the flash lamps operate in the absence of a triggering particle. For the present mission, several minutes of forced trigger data were collected prior to each flight and we take the average value plus nine standard deviations ( $9\sigma$ ) as the threshold above which a particle is considered “fluorescent” in each channel. Although a number of earlier papers used a lower threshold of  $3\sigma$  (Crawford et al., 2017; Toprak & Schnaiter, 2013), we follow the recommendations put forth by Savage et al. (2017) intended to minimize possible non-biological interferences, which often exhibit less intense fluorescence. For example, Savage et al. (2017) find that both dust and humic materials are effectively rejected when a higher fluorescence threshold is used. Certain kinds of black carbon are fluorescent enough to be categorized as fluorescent even with the higher threshold, however size distributions for those particles tend to peak at smaller diameters than is observed for most ambient PBA. We note that this higher threshold complicates comparisons to previously reported fluorescent concentrations and we therefore include Figures S3 and S4 in Supporting Information S1 showing concentrations calculated based on the lower threshold, for transparency and to facilitate comparison. With this data processing strategy, we believe it is unlikely that a substantial portion of our observed fluorescent particles were anthropogenic in nature as evidenced by their size, spectral signature and the remoteness of the location.

The optical sizing of the WIBS was calibrated before and after the mission using commercial monodisperse polystyrene latex (PSL) spheres and fitting to Mie theory calculations as described in Perring et al. (2015). As

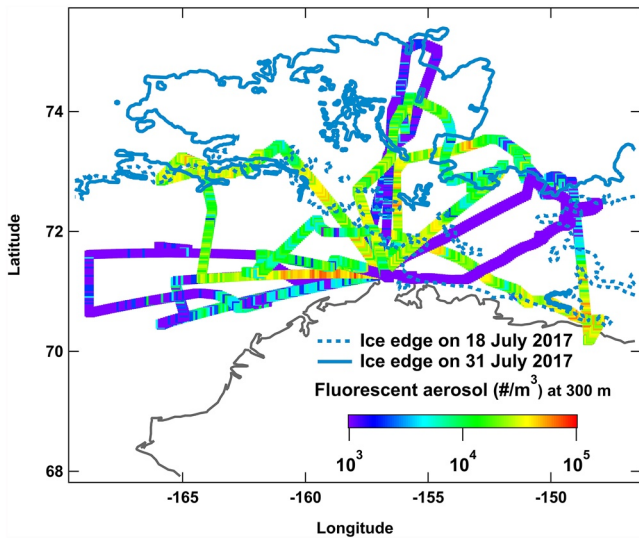


**Figure 1.** Map of flight tracks colored by fluorescent aerosol concentrations. Also marked are ice-edge boundaries at the beginning (dashed blue line) and end (solid blue line) of the campaign.

reported in Robinson et al. (2017) there is a flow rate dependence to the sizing calibration, presumably arising from inadequate temporal resolution in the scattering signal detection. For the present mission the sample flow was 0.5 LPM and the sheath flow was 1.5 LPM; this is a lower-than-typical sheath to sample ratio, chosen to minimize the flow velocity through the jet (determined by the sum of sheath and sample flow rates) while maximizing the volume of air sampled to improve statistics in a low-particle environment. The gain on the scattering detector was increased relative to the typical WIBS configuration such that the instrument used here detected particles from roughly 0.5–10  $\mu\text{m}$ . To investigate the detection efficiency at small sizes, the WIBS and a Portable Optical Particle Sensor (POPS, Handix Scientific, Boulder CO) sampled simultaneously from a well-mixed container into which PSL spheres of various submicron sizes were introduced. The particle concentrations reported by the two instruments matched to within 5% for sizes down to  $\sim 0.4 \mu\text{m}$ . We take this as evidence that the WIBS is a reliable particle counter in the size range presented here and use it as a counter of both fluorescent and total aerosol in our analysis. We note that there is a separate, unanswered question as to whether the amount of fluorescent material in a typical, ambient, small particle would be detectable to the WIBS thus we may be underestimating concentrations of small, weakly fluorescent PBA.

The fluorescence response in channels A and B was calibrated according to methods outlined in Robinson et al. (2017) using polydisperse quinine prior to the mission and using size-selected particles of quinine and mixed tryptophan in ammonium sulfate after the mission. The pre- and post-mission quinine calibrations agreed well and the mass-equivalent response was 1.3 counts/fg quinine in FL1 and 0.54 counts/fg quinine in FL2. This corresponds to minimum detectable quinine masses of approximately 80 and 340 fg in FL1 and FL2 respectively, depending on the background in each channel for a particular flight.

## 2.2. Lidar

Lidar results from this study have been published in Churnside et al. (2020) and the detection methodology is discussed in more detail in Churnside and Marchbanks (2015) and Churnside et al. (2021). Briefly, the instrument transmits 12 ns pulses of linearly polarized 532 nm light at 30 Hz and detects copolarized and cross polarized backscatter from the ocean with a sample rate of 1 GHz and a depth resolution of  $\sim 1$  m. For this work, we used the lidar attenuation coefficient,  $\alpha$ , from the cross-polarized return when the flight altitude was 300 m. This was calculated from the slope of the logarithm of the signal versus depth over the depth range where the log signal was linear. This parameter very nearly approximates the diffuse attenuation coefficient, which is proportional to the chlorophyll concentration in the upper mixed layer. Because of this relationship, we used  $\alpha$  as a proxy for productivity in the upper ocean.

Due to the large difference in reflectivity between ice and open water, the lidar was able to determine the fraction of the surface that was covered by ice by counting the fraction of lidar shots exceeding a particular threshold in each kilometer of flight track. The surface is commonly considered to be open water when the fraction is  $<15\%$ , broken ice when the fraction is  $15\text{--}80\%$  and pack ice when the fraction is  $>80\%$  (Dumont, 2022). Since the return from ice generally saturated the detector, the result was insensitive to the threshold chosen. No information about the ocean was obtained from the lidar shots that hit ice, but the narrow beam easily penetrated between ice to provide estimates of  $\alpha$  even in ice fractions  $>90\%$ .

## 2.3. Mission Description and Sampling Strategy

This campaign was based out of Utqiagvik, AK during the month of July in 2017. Flight tracks (Figure 1) were chosen to sample from a variety of surface ice coverage conditions and also to cover as wide a geographic area as possible given aircraft range limitations. See Churnside et al. (2020) for a description of ice extent over the course of the project. Most flights targeted clear air to facilitate lidar retrievals. The majority of flight time was spent at



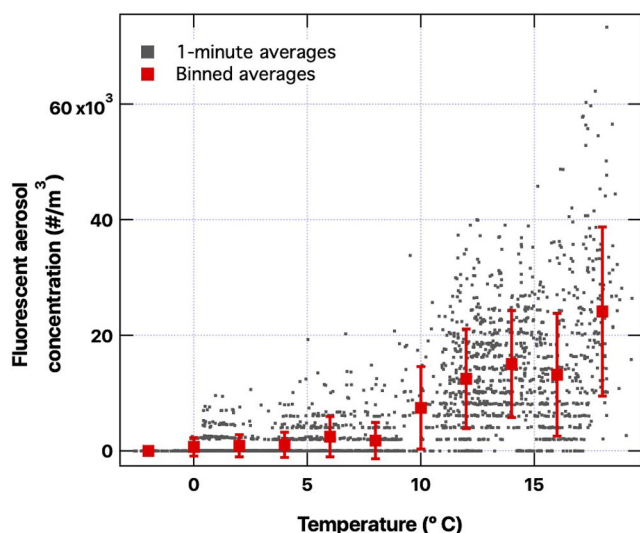


**Figure 2.** Observed  $>1 \mu\text{m}$  fluorescent aerosol concentrations versus ambient temperature. Small gray symbols represent 1-min average concentrations observed at 300 m while red squares with error bars represent binned means and standard deviations calculated for 2-degree temperature windows.

300 m above the surface, the optimal height for lidar retrievals, with occasional stacked profiles (1 or 2 per flight) performed to probe in situ aerosol at higher and lower altitudes (900 and 60 m respectively). Profile locations were determined in-flight based on lidar observations and selected to span a variety of surface ocean productivity levels. When a particular location was chosen for a profile, the pilots descended from 300 m while turning and flew back along the most recent trajectory at 60 m for 5 min. After the lower leg, the plane ascended to 900 m and turned to overfly the original track for another 5 min before descending back to 300 m to continue the rest of the flight. Although we did not assess the local boundary layer height directly, previous work from a similar region and season (Brooks et al., 2017) indicates that 60 m should be well within the marine boundary layer, 300 m may be within it or slightly above it and 900 m should be well above the marine boundary layer. We discuss how our measurements and calculations constrain the marine boundary layer height in further detail in the results section below.

The inlet used for sampling of in situ aerosol was designed to optimize aspiration and transmission of large aerosol under the flight conditions of the Twin Otter at a specified airspeed of 100 mph (44.7 m/s). The total calculated efficiency was better than 80% for sizes from our lower limit of detection of 0.5–5.4  $\mu\text{m}$  with a 50% cutoff size of  $\sim 8.8 \mu\text{m}$  and falling to 35% at 10  $\mu\text{m}$ . The inlet consisted of a forward-facing dual diffuser inlet as described by Schwarz et al. (2006) which was mounted on the forward starboard window

at a  $10^\circ$  downward angle, determined experimentally to be parallel with the airflow around the fuselage at that location. The primary diffuser consisted of a smaller forward opening followed by an expansion and a larger rear opening such that the flow velocity at the tip of the diffuser was isokinetic with external airflow and the flow velocity within the diffuser was reduced by a factor of  $\sim 50$ . The secondary diffuser sampled from within the primary diffuser and resulted in an additional reduction in flow velocity. For the present configuration, flow through the secondary diffuser was actively controlled at 0.68 L/min and the internal diameter of the secondary diffuser was chosen such that it was operating isokinetically with the flow within the primary diffuser. Stainless steel tubing was used to connect the inlet to the WIBS and losses during transport were minimized by minimizing horizontal transport distance and bends and by striving to reduce turbulence as much as possible at all joints.

### 3. Results

#### 3.1. General Characteristics of Fluorescent Particle Populations

Observed concentrations of fluorescent aerosol were highly variable (Figure 1). On about half of the flights, observed concentrations at 300 m were  $1 \times 10^4 \text{ m}^{-3}$  or more while, on other flights, loadings were an order of magnitude lower. The high-concentration regime had fluorescent particle loadings similar to those observed over the continental US at a similar altitude (Perring et al., 2015) where regional concentrations varied from 2 to  $8 \times 10^4 \text{ m}^{-3}$ . Note that the previous study used a  $3\sigma$  threshold for determining fluorescence so those loadings would be reduced if processed to match the present analysis. These high- and low-concentration regimes typically persisted for large fractions of flights and there was no discernible spatial pattern to where higher and lower loadings were observed. Taken together, we interpret this to mean that the observed concentrations were driven by regional phenomena rather than individual emission sources strongly impacting a particular area. In contrast to the lack of spatial patterns, there was a strong correspondence between observed fluorescent aerosol loadings and air temperature (Figure 2) whereby higher temperatures corresponded to higher loadings. This led to the hypothesis that airmasses with high loadings had been advected from the boundary layer of terrestrial ecosystems where surface temperatures were high, and those with low loadings either originated from marine environments where surface temperatures were closer to  $0^\circ\text{C}$  or had been transported at high altitudes (above the planetary boundary layer) for some time. This hypothesis is investigated in more detail in Section 3.3 using back trajectory analysis.

Figure 3 shows two example profiles, the left from 18 July when loadings at 300 m were relatively low and the right from 28 July when loadings at 300 m were relatively high. The lower legs of both profiles are similar and exemplary of nearly every 60 m leg flown: they have high total aerosol loadings and low fluorescent

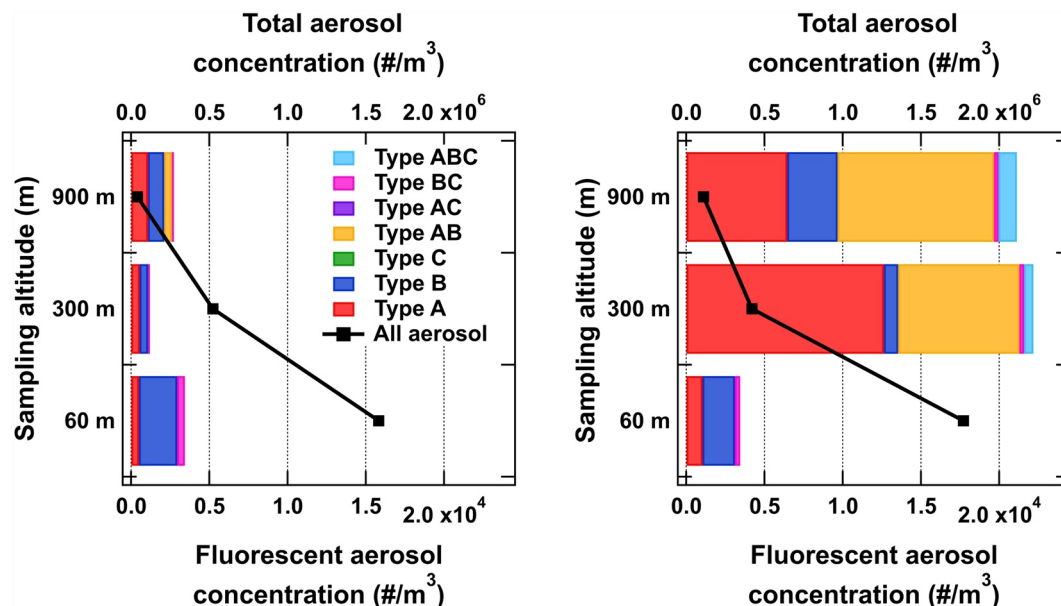


**Figure 3.** Example vertical profiles of fluorescent (colored, stacked bars, bottom axes) and total (black squares and lines, top axes) aerosol concentrations from 18 July 2017 (left) and 28 July 2017 (right). Back trajectories indicate no terrestrial influence for the left profile but strong terrestrial influence for the right profile at the two higher altitudes.

aerosol loadings and the majority of the observed fluorescent aerosol is type B. It was also nearly always the case that the air temperature at 60 m was close to 0°C even when it was much warmer aloft. In fact, out of 12 profiles performed, only one had elevated fluorescent concentrations ( $>5 \times 10^3 \text{ m}^{-3}$ ) at 60 m and that profile also occurred quite close to shore and had an elevated air temperature, likely indicating a terrestrial influence (see 31 July profile in Figure S2 in Supporting Information S1). We take the stark increase in total particle loads and uniformly low temperatures at the lowest sampling altitudes to indicate that we were usually sampling within the marine boundary layer where one would expect to find abundant wind-generated sea spray aerosol and air temperatures that mirror that of the water/ice surface. In addition, on days when the temperature at 300 m was substantially above that at 60 m, it is reasonable to assume that the top of the boundary layer must lie somewhere between 60 and 300 m placing the lowest altitude within the marine boundary layer and the two higher altitudes above it. On days when the temperature at 300 m was close to that observed at 60 m, it is possible that 300 m was within the marine boundary layer. The fluorescent loadings at 60 m reported here are lower than another recent report from within the MBL at lower latitudes (Kawana et al., 2021) and inconsistent with high observed concentrations of warm temp IN within the MBL at a different location in the Arctic during the same summer (Creamean et al., 2018). This likely indicates that there is not a strong source of fluorescent aerosol from the ocean surface at the time of our sampling, a hypothesis which is explored in more detail in Section 3.2.

The two profiles in Figure 3 differ markedly in the observations at the two upper altitudes. On 18 July, fluorescent loadings and observed types at 300 and 900 m are similar to those observed at 60 m while on 28 July the loadings at 300 and 900 m are much higher and the fluorescent types observed are predominantly type A and AB. Note also the similarity in terms of fluorescent concentration and type distribution between the 300 and 900 m legs. This was consistent across the data set; of five profiles that had elevated concentrations at both levels the concentrations observed at 900 m were, on average, 7% less than those observed at 300 m. A sixth profile had elevated concentrations only at 900 m while the remaining profiles exhibited concentrations similar to those observed in the MBL. Thus, we believe that the elevated fluorescent aerosol layer, when present, usually extended vertically from the top of the MBL to at least 900 m in addition to having a broad spatial extent.

Figure 4 shows number distributions for total aerosol and fluorescent aerosol observed at 300 m (both from WIBS data) when temperatures aloft were  $>10^\circ\text{C}$  (left) and below  $5^\circ\text{C}$  (right) including data from the whole campaign. On days with warmer temperatures at 300 m, the number distributions of types A, AB, and ABC appear similar to those observed in laboratory studies of fungal spores (Hernandez et al., 2016). There is also a minor population of type B particles, peaking around  $2 \mu\text{m}$ , that is not similar to laboratory observations of known bioaerosol, but

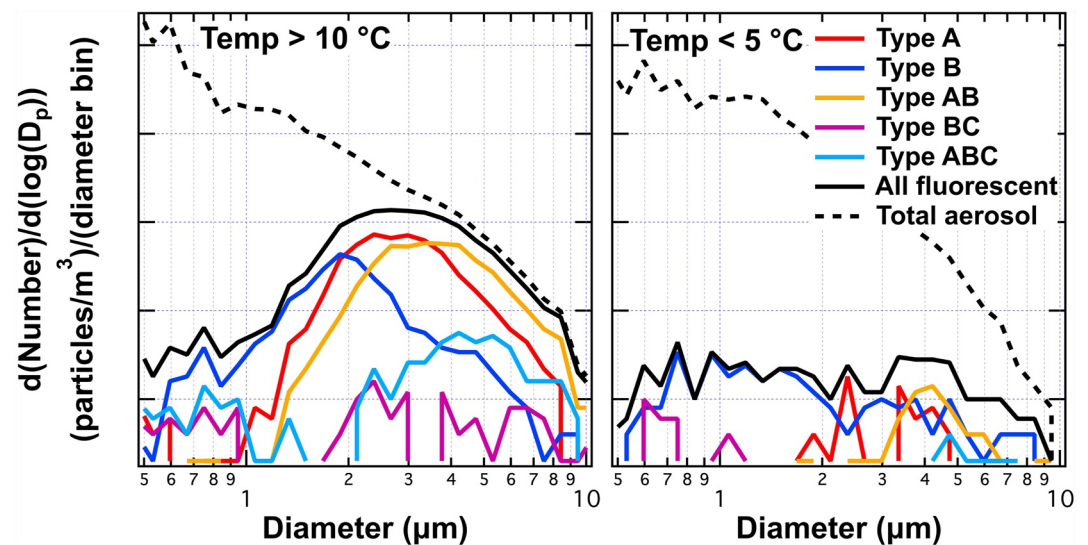


**Figure 4.** Number distributions of fluorescent particles (solid lines) and total aerosol (dashed lines) observed at 300 m altitude for temperatures above 10°C (left) and below 5°C (right).

which is similar to previous observations of fluorescent aerosol in the marine boundary layer at lower latitudes reported by Kawana et al. (2021). On days with cooler temperatures at 300 m, the type B particles are dominant and appear at slightly smaller sizes. We do not have enough information to theorize as to the identity of these particles but it is possible that they are characteristic of some marine source, as posited by Kawana et al. (2021) through observed correlations with bacteria and biogenic gel organic particles. We note that, on warmer days, type B particles account for a minor fraction of the total fluorescent aerosol number; they are included in our analysis for completeness. On warm days, fluorescent aerosol accounted for ~12% of supermicron aerosol number and 64% of supermicron aerosol volume while, on cooler days, fluorescent aerosol accounted for only 0.2% of supermicron aerosol number and 7% of volume.

### 3.2. Assessing Oceanic Emissions of Fluorescent Aerosol

Numerous papers have reported observations that imply the surface ocean, either the sea surface microlayer or particular marine organisms, can be a source of biological aerosol (Burrows et al., 2013; DeMott et al., 2016; Knopf et al., 2011; McCluskey et al., 2018; Moallemi et al., 2021; Santander et al., 2021). Findings are mixed as to the size range of particle produced, their fluorescent signature and their ice nucleation activity.

Here we use our observations of fluorescent aerosol within the MBL, in conjunction with the lidar data regarding subsurface layers of biological activity to evaluate potential emissions of biological aerosol from the Arctic Ocean. The left panel of Figure 5 shows the relationship between total fluorescent aerosol concentration measured by the WIBS and lidar attenuation colored by the ice fraction of the flight segment in question. Each data point represents an average of a single leg at 60 m altitude, typically about 5 min of flight time. There is no systematic relationship observed between the fluorescent aerosol concentration and  $\alpha$ . We also examined the relationship between  $\alpha$  and the fluorescent fraction (right panel of Figure 5), since absolute concentrations would likely be a function of both PBA concentrations in the surface layer and wind speed; we find a similar lack of correspondence in that case as well. Thus we observe no relationship between biological activity in the surface ocean and enhancements of fluorescent aerosol in the adjacent marine boundary layer.

To give context for this observation we can compare to a couple of recent studies. First, Kawana et al. (2021) measured fluorescent aerosol during a cruise in the Pacific Ocean that spanned a range of lower latitudes between 35°N and 20°S. They observed fluorescent aerosol loadings of 10–40 per liter during the oceanically-influenced portion of their cruise, concentrations that are an order of magnitude higher than those reported here for the Arctic MBL. We note that, even considering the brevity of our excursions to the lowest altitude, the concentrations reported in Kawana et al. (2021) would be easily detectable to our instrument and we can say with

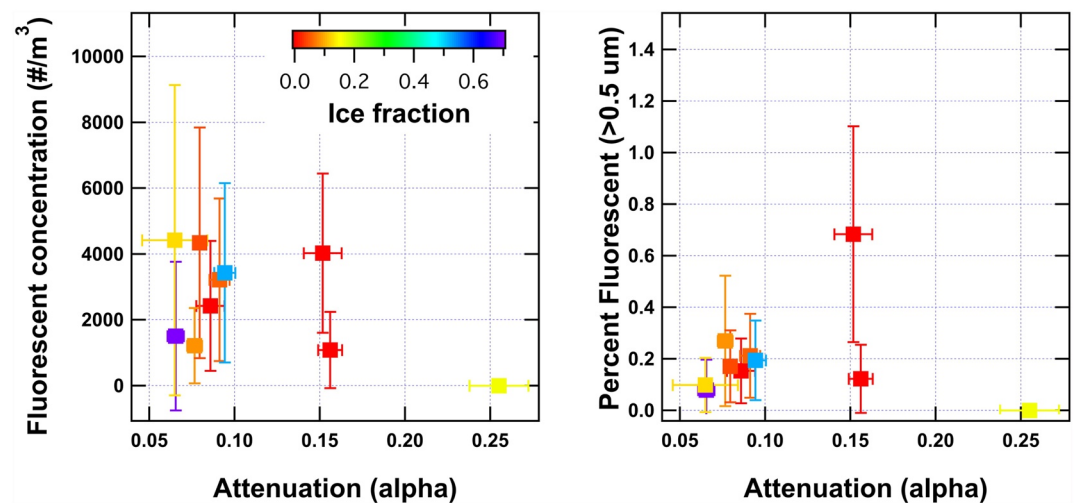


**Figure 5.** The fluorescent aerosol concentration (left) and percent (right) observed at 60 m altitude versus lidar attenuation, colored by ice fraction. Vertical error bars represent standard deviations for 1 s WIBS measurements and horizontal error bars represent standard deviations for the corresponding lidar measurements.

confidence that our observations are significantly different, likely due to the latitudinal difference between the two studies. Second, Creamean et al. (2019) report elevated IN activity measured in coarse-mode aerosol samples in association with the presence of subsurface phytoplankton layers. These observations were made in the Arctic, at a slightly different location and later in the summer as compared to the measurements we discuss here. The most active samples had IN concentrations of  $>10^{-4} \text{ L}^{-1}$  at  $-10^{\circ}\text{C}$  and  $\sim 3 \times 10^{-3} \text{ L}^{-1}$  at  $-15^{\circ}\text{C}$ . If we use an IN parameterization published by Tobo et al. (2013) to estimate IN concentrations in the MBL for the present study based on observed fluorescent aerosol concentrations, we find that the IN concentrations one would expect are a factor of  $\sim 5$  lower than those observed by Creamean et al. (2019). We note that this parameterization was developed for a mid-latitude forest ecosystem that may not be applicable to the Arctic environment, however we still find it striking that we saw such low concentrations of fluorescent aerosol in the marine boundary layer. Thus, while it seems likely that oceanic emissions of PBA in the Arctic occur episodically and/or in particular locations, we can say with reasonable confidence that we did not observe that behavior in the area of our sampling. Perhaps our sampling corresponded to cooler sea surface temperatures than seen in other studies or, although we primarily targeted areas of clear air, it is possible that cloud scavenging had occurred prior to our sampling within the marine boundary layer. Another potential explanation is that some studies report IN enhancements from decaying phytoplankton blooms as opposed to active blooms (McCluskey et al., 2018; Zeppenfeld et al., 2019), in which case, we might not have been targeting appropriate areas within the MBL for sampling.

### 3.3. Assessing Terrestrial Emissions of Fluorescent Aerosol

Here we use the NOAA HYSPLIT model (Draxler, 1999; Draxler & Hess, 1997, 1998; Stein et al., 2015) to investigate the source of elevated fluorescent aerosol concentrations above the Arctic Ocean. 10-day back trajectories were calculated using meteorology from the  $1^{\circ}$  GDAS meteorological data set with modeled vertical velocity. Estimates of boundary layer height and precipitation were also extracted along the trajectory and daytime marine boundary layer heights are generally estimated to be less than 500 m, in agreement with the literature (Brooks et al., 2017). First, to evaluate our hypothesis of a dominant terrestrial source, we chose two flight days that showed strong contrast in observed fluorescent concentrations and ran back trajectories from the aircraft location every 5 min for each of the two flights. On 27 July we observed relatively cool temperatures and low concentrations of fluorescent aerosol above the MBL, while on July 28th we observed warmer temperatures and enhanced concentrations of fluorescent aerosol. The back trajectories show broad similarities between the general air mass origins for both days, with both primarily receiving transport from the south and west of the study location (Figure 6, top panels), however, there was a strong difference between the 2 days in the locations of boundary layer interceptions (Figure 6, bottom panels) defined as instances when the back trajectory altitude was less than the calculated boundary layer height. On the day with elevated fluorescent concentrations aloft (28 July, left



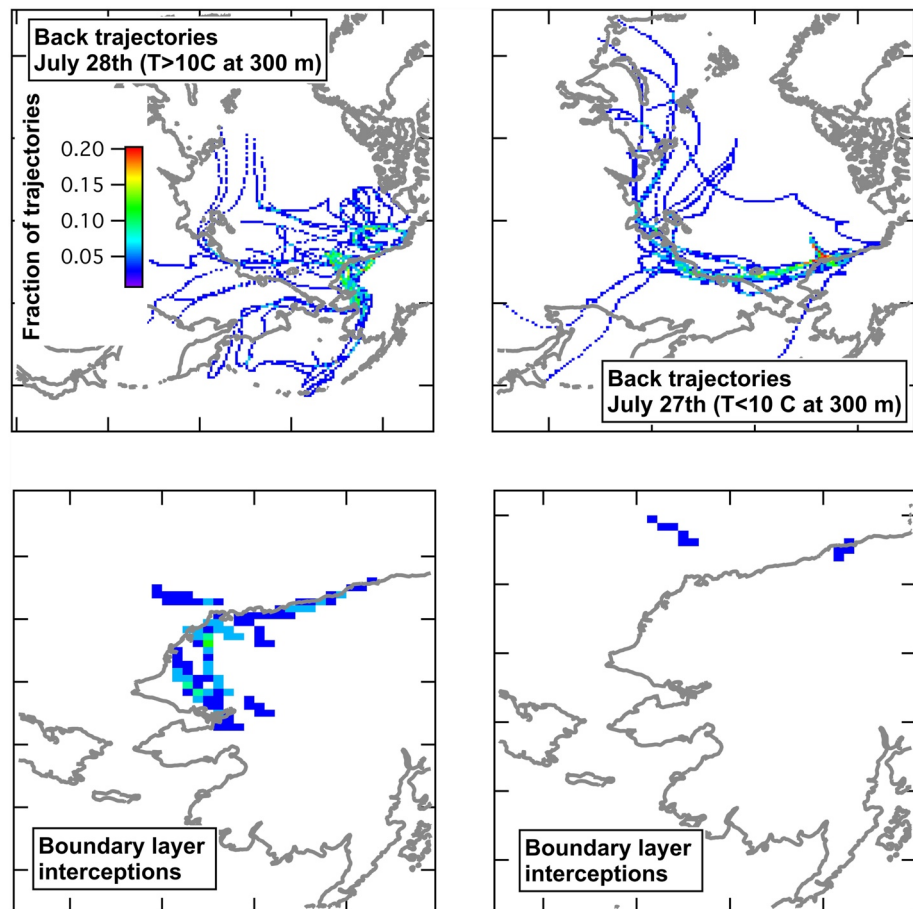


**Figure 6.** Back trajectory results from flights on 28 July (left column) and 27 July (right column). The top row shows 10-day trajectories regardless of altitude, the bottom row shows the locations of calculated boundary layer interceptions within the two most recent days.

column) there are numerous recent boundary layer interceptions over land while, on the other day (27 July, right column), there is minimal interaction with the boundary layer and the few interceptions that do occur happen over the ocean, thus lending credence to our hypothesis of a terrestrial source for the observed fluorescent particles.

Next, we ran a more statistically meaningful set of back trajectories for the whole project in which we initiated a trajectory whenever there were at least 10 min of level flight within 15 min of the top of the hour. This ensured that there was a good temporal match between the GDAS meteorology and the observations used and that we had no duplicate trajectories (as would happen if one were to initiate multiple trajectories within the same  $1^\circ$  spatial bin for the same GDAS time step). For each trajectory, we recorded the number of hours in the most recent 2 days for which the modeled air parcel altitude was below the estimated boundary layer height and calculated the average boundary layer height for that set of time points. We can then calculate an emissions rate as follows:

$$E = [\overline{\text{FAP}}]_{\text{obs}} * \overline{H}_{\text{BL}} / \Sigma(\text{Hrs})_{\text{BL}}$$

where  $[\overline{\text{FAP}}]_{\text{obs}}$  is the observed average fluorescent aerosol particle concentration at the point of sampling,  $\overline{H}_{\text{BL}}$  is the average boundary layer height calculated when the air parcel was in the boundary layer and  $\Sigma(\text{Hrs})_{\text{BL}}$  is the number of hours spent in the boundary layer. Figure 7 shows the resulting emissions estimate plotted as a function of temperature at the point of sampling considering boundary layer interceptions within the most recent 48 hr. Also shown are averages for 4-degree temperature bins calculated considering interceptions within the most recent 48, 72, 96, and 240 hr. For this calculation we include only types A, AB, and ABC in  $\text{FAP}_{\text{obs}}$  as those are the particles that appear similar to known biological aerosol, though we note that including all fluorescent particles would only increase the estimated emissions by  $\sim 12\%$ . The resulting emissions estimates are comparable

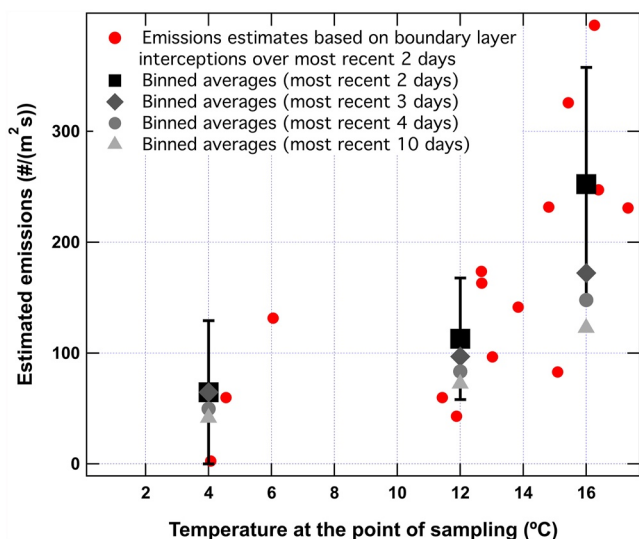


**Figure 7.** Estimated emission rates of fluorescent aerosol from Arctic terrestrial environments as a function of temperature at the point of sampling. Red circles show emission rates based on analysis of individual trajectories. Black squares and bars show average inferred emission rates and standard deviations calculated for 4° temperature bins.

to, or higher than, modeled summertime emissions rates of fungal spores in the continental US. (Janssen et al., 2021) This finding is especially interesting since models (which are often tied to leaf area index) would not predict strong PBA sources in the Arctic, even in the summer.

### 3.4. The Potential Effects of Interferences

It is important to consider potential non-biological interferences in the context of these results. Previous studies have shown that dust contributes a substantial fraction of fluorescent particle loadings in remote environments (Crawford et al., 2016; D. Morrison et al., 2020). Crawford et al. (2016) used a lower fluorescence threshold than we use here, so we are likely detecting a substantially smaller fraction of those particles. D. Morrison et al. (2020) used the same fluorescence threshold as the one used here and still found a large fraction of fluorescence from dust, however they were sampling dust plumes near Cape Verde which is a substantially different environment than the Arctic. We are unable to conclusively state that dust is not contributing to our signal, however, we note that the correspondence with temperature is a relationship that would be expected for biological systems but not for dust emissions.

Similarly, black carbon is known to produce fluorescent signals in the WBS (Perring et al., 2015; Savage et al., 2017). The particular type presentation (A or B) depends on the black carbon source, however the corresponding size distribution typically peaks at smaller sizes (<1 μm) as compared to those observed here. Creamean et al. (2018) report a dominant influence of regional biomass burning aerosol in our sampling region during summer of 2015, however we checked MODIS hot spot data for July 2017 and did not find fires in regions identified in our back trajectory analysis. Although there are local sources of anthropogenic black carbon, particularly the Prudhoe Bay oilfield (Creamean et al., 2018; Gansch et al., 2017; Maahn et al., 2017), only a minority of our back trajectories pass through that region. In the absence of specific local sources or particular transport events, other researchers report that natural aerosols dominate the Arctic in the summertime and that anthropogenic aerosol becomes more important in the winter (e.g., Moschos et al., 2022; Quinn et al., 2009). Finally, as with the potential for a mineral dust interference, we would not expect local or transported black carbon concentrations to show the positive correlation with temperature that we observe.

In summary, we have attempted to minimize non-biological fluorescent interferences as much as possible in both our sampling and data processing methods. We find no evidence that the sampled air is substantially impacted by emissions of such particles and we believe that these results are valuable and interesting, even if we accept that a fraction of our observed signal may arise from unknown interferences.

## 4. Conclusions

Here we report airborne measurements of fluorescent aerosol, which we use as a proxy for PBA, collected over the Arctic Ocean during the summer of 2017. Observed loadings varied greatly from day-to-day and the highest loadings approached those observed previously over the continental US. Measurements were made most often at 300 m above the ocean surface with occasional excursions to 60 and 900 m to investigate vertical distributions. Fluorescent aerosol loadings were always very low at the lowest altitude and showed no systematic relationship to lidar measurements of sub-surface biological productivity, which we take to mean that there were no appreciable oceanic emissions of fluorescent aerosol at the time and location of our sampling. Fluorescent aerosol loadings at the two higher altitudes showed a strong positive correlation with air temperature and calculated back trajectories indicate a terrestrial source for the particles. We then further used the back trajectories to estimate emission rates of fluorescent aerosol from the Arctic tundra, finding rates comparable to those recently estimated for fungal spores in the summertime continental US. We believe that this is an unappreciated source of biological aerosol to the Arctic free troposphere which may be rapidly growing as the Arctic warms due to climate change. These findings could have strong implications for regional clouds and, in turn, the Arctic radiation budget, especially in the summer and early fall.

## Data Availability Statement

The data set from this project, titled “Fluorescent Aerosol and Meteorological data over the Chukchi and Beaufort Seas, July 2017,” has been archived with the National Center for Environmental Information under accession number 0277794 (Perring et al., 2023).

## Acknowledgments

The work reported here was supported by the NOAA Atmospheric Composition and Climate Program and the NOAA Health of the Atmosphere Program. AEP, GDW, and BM also acknowledge the Colgate Research Council for funding. The authors are grateful to the NOAA Twin Otter pilots, Shanae Coker and Frank Centinello III, and mechanic, Robert Miletic, for their important contributions.

## References

- Bigg, E. K., & Leck, C. (2001). Cloud-active particles over the central Arctic Ocean. *Journal of Geophysical Research*, *106*(D23), 32155–32166. <https://doi.org/10.1029/1999JD901152>
- Brooks, I. M., Tjernström, M., Persson, P. O. G., Shupe, M. D., Atkinson, R. A., Canut, G., et al. (2017). The turbulent structure of the Arctic summer boundary layer during the Arctic summer cloud-ocean study. *Journal of Geophysical Research: Atmospheres*, *122*(18), 9685–9704. <https://doi.org/10.1002/2017JD027234>
- Burrows, S. M., Hoose, C., Pöschel, U., & Lawrence, M. G. (2013). Ice nuclei in marine air: Biogenic particles or dust? *Atmospheric Chemistry and Physics*, *13*(1), 245–267. <https://doi.org/10.5194/acp-13-245-2013>
- Christner, B. C., Morris, C. E., Foreman, C. M., Cai, R., & Sands, D. C. (2008). Ubiquity of biological ice nucleators in snowfall. *Science*, *319*(5867), 1214. <https://doi.org/10.1126/science.1149757>
- Churnside, J. H., & Marchbanks, R. D. (2015). Subsurface plankton layers in the Arctic Ocean. *Geophysical Research Letters*, *42*(12), 4896–4902. <https://doi.org/10.1002/2015GL064503>
- Churnside, J. H., Marchbanks, R. D., & Marshall, N. (2021). Airborne lidar observations of a spring phytoplankton bloom in the western Arctic Ocean. *Remote Sensing*, *13*(13), 2512. Article 13. <https://doi.org/10.3390/rs13132512>
- Churnside, J. H., Marchbanks, R. D., Vagle, S., Bell, S. W., & Stabeno, P. J. (2020). Stratification, plankton layers, and mixing measured by airborne lidar in the Chukchi and Beaufort seas. *Deep-Sea Research Part II: Topical Studies in Oceanography*, *177*, 104742. <https://doi.org/10.1016/j.dsr2.2020.104742>
- Crawford, I., Gallagher, M. W., Bower, K. N., Choularton, T. W., Flynn, M. J., Ruske, S., et al. (2017). Real-time detection of airborne fluorescent bioparticles in Antarctica. *Atmospheric Chemistry and Physics*, *17*(23), 14291–14307. <https://doi.org/10.5194/acp-17-14291-2017>
- Crawford, I., Loyd, G., Herrmann, E., Hoyle, C. R., Bower, K. N., Connolly, P. J., et al. (2016). Observations of fluorescent aerosol–cloud interactions in the free troposphere at the High-Altitude Research Station Jungfraujoch. *Atmospheric Chemistry and Physics*, *16*(4), 2273–2284. <https://doi.org/10.5194/acp-16-2273-2016>
- Creamean, J. M., Cross, J. N., Pickart, R., McRaven, L., Lin, P., Pacini, A., et al. (2019). Ice nucleating particles carried from below a phytoplankton bloom to the Arctic Atmosphere. *Geophysical Research Letters*, *46*(14), 8572–8581. <https://doi.org/10.1029/2019GL083039>
- Creamean, J. M., Kirpes, R. M., Pratt, K. A., Spada, N. J., Maahn, M., de Boer, G., et al. (2018). Marine and terrestrial influences on ice nucleating particles during continuous springtime measurements in an Arctic oilfield location. *Atmospheric Chemistry and Physics*, *18*(24), 18023–18042. <https://doi.org/10.5194/acp-18-18023-2018>
- Creamean, J. M., Suski, K. J., Rosenfeld, D., Cazorla, A., DeMott, P. J., Sullivan, R. C., et al. (2013). Dust and biological aerosols from the Sahara and Asia influence precipitation in the western U.S. *Science*, *339*(6127), 1572–1578. <https://doi.org/10.1126/science.1227279>
- Dai, H. (2021). Roles of surface Albedo, surface temperature and carbon dioxide in the seasonal variation of Arctic Amplification. *Geophysical Research Letters*, *48*(4), e2020GL090301. <https://doi.org/10.1029/2020GL090301>
- DeMott, P. J., Hill, T. C. J., McCluskey, C. S., Prather, K. A., Collins, D. B., Sullivan, R. C., et al. (2016). Sea spray aerosol as a unique source of ice nucleating particles. *Proceedings of the National Academy of Sciences of the United States of America*, *113*(21), 5797–5803. <https://doi.org/10.1073/pnas.1514034112>
- DeMott, P. J., & Prenni, A. J. (2010). New Directions: Need for defining the numbers and sources of biological aerosols acting as ice nuclei. *Atmospheric Environment*, *44*(15), 1944–1945. <https://doi.org/10.1016/j.atmosenv.2010.02.032>
- Draxler, R. R. (1999). *HYSPLIT4 user's guide*. NOAA Technical Memorandum ERL ARL-230, NOAA Air Resources Laboratory.
- Draxler, R. R., & Hess, G. D. (1997). *Description of the HYSPLIT\_4 modeling system* (p. 24). NOAA Technical Memorandum ERL ARL-224, NOAA Air Resources Laboratory, Silver Spring, MD.
- Draxler, R. R., & Hess, G. D. (1998). *An overview of the HYSPLIT\_4 modeling system of trajectories, dispersion, and deposition* (Vol. 47, pp. 295–308). Australian Meteorological Magazine.
- Dumont, D. (2022). Marginal ice zone dynamics: History, definitions and research perspectives. *Philosophical Transactions. Series A, Mathematical, Physical, and Engineering Sciences*, *380*(2235), 20210253. <https://doi.org/10.1098/rsta.2021.0253>
- Fröhlich-Nowoisky, J., Kampf, C. J., Weber, B., Huffman, J. A., Poehlker, C., Andreae, M. O., et al. (2016). Bioaerosols in the Earth system: Climate, health, and ecosystem interactions. *Atmospheric Research*, *182*, 346–376. <https://doi.org/10.1016/j.atmosres.2016.07.018>
- Gabey, A. M., Gallagher, M. W., Whitehead, J., Dorsey, J. R., Kaye, P. H., & Stanley, W. R. (2010). Measurements and comparison of primary biological aerosol above and below a tropical forest canopy using a dual channel fluorescence spectrometer. *Atmospheric Chemistry and Physics*, *10*(10), 4453–4466. <https://doi.org/10.5194/acp-10-4453-2010>
- Gong, T., Feldstein, S., & Lee, S. (2017). The role of downward infrared radiation in the recent Arctic winter warming trend. *Journal of Climate*, *30*(13), 4937–4949. <https://doi.org/10.1175/JCLI-D-16-0180.1>
- Gunsch, M. J., Kirpes, R. M., Kolesar, K. R., Barrett, T. E., China, S., Sheesley, R. J., et al. (2017). Contributions of transported Prudhoe Bay oil field emissions to the aerosol population in Utqiagvik, Alaska. *Atmospheric Chemistry and Physics*, *17*(17), 10879–10892. <https://doi.org/10.5194/acp-17-10879-2017>
- Hartmann, M., Adachi, K., Eppers, O., Haas, C., Herber, A., Holzinger, R., et al. (2020). Wintertime Airborne measurements of ice nucleating particles in the high Arctic: A hint to a marine, biogenic source for ice nucleating particles. *Geophysical Research Letters*, *47*(13), e2020GL087770. <https://doi.org/10.1029/2020GL087770>
- Hartmann, M., Gong, X., Kecorius, S., van Pinxteren, M., Vogl, T., Welti, A., et al. (2021). Terrestrial or marine—Indications towards the origin of ice-nucleating particles during melt season in the European Arctic up to 83.7°N. *Atmospheric Chemistry and Physics*, *21*(15), 11613–11636. <https://doi.org/10.5194/acp-21-11613-2021>
- Healy, D. A., O'Connor, D. J., Burke, A. M., & Sodeau, J. R. (2012). A laboratory assessment of the Waveband Integrated Bioaerosol Sensor (WIBS-4) using individual samples of pollen and fungal spore material. *Atmospheric Environment*, *60*, 534–543. <https://doi.org/10.1016/j.atmosenv.2012.06.052>
- Hernandez, M., Perring, A. E., McCabe, K., Kok, G., Granger, G., & Baumgardner, D. (2016). Chamber catalogues of optical and fluorescent signatures distinguish bioaerosol classes. *Atmospheric Measurement Techniques*, *9*(7), 3283–3292. <https://doi.org/10.5194/amt-9-3283-2016>

- Huffman, J. A., Prenni, A. J., DeMott, P. J., Poehlker, C., Mason, R. H., Robinson, N. H., et al. (2013). High concentrations of biological aerosol particles and ice nuclei during and after rain. *Atmospheric Chemistry and Physics*, *13*(13), 6151–6164. <https://doi.org/10.5194/acp-13-6151-2013>
- Hwang, Y.-T., Frierson, D. M. W., & Kay, J. E. (2011). Coupling between Arctic feedbacks and changes in poleward energy transport. *Geophysical Research Letters*, *38*(17), L17704. <https://doi.org/10.1029/2011GL048546>
- Janssen, R. H. H., Heald, C. L., Steiner, A. L., Perring, A. E., Huffman, J. A., Robinson, E. S., et al. (2021). Drivers of the fungal spore bioaerosol budget: Observational analysis and global modeling. *Atmospheric Chemistry and Physics*, *21*(6), 4381–4401. <https://doi.org/10.5194/acp-21-4381-2021>
- Kawana, K., Matsumoto, K., Taketani, F., Miyakawa, T., & Kanaya, Y. (2021). Fluorescent biological aerosol particles over the central Pacific Ocean: Covariation with ocean surface biological activity indicators. *Atmospheric Chemistry and Physics*, *21*(20), 15969–15983. <https://doi.org/10.5194/acp-21-15969-2021>
- Kaye, P. H., Stanley, W. R., Hirst, E., Foot, E. V., Baxter, K. L., & Barrington, S. J. (2005). Single particle multichannel bio-aerosol fluorescence sensor. *Optics Express*, *13*(10), 3583–3593. <https://doi.org/10.1364/OPEX.13.003583>
- Knopf, D. A., Alpert, P. A., Wang, B., & Aller, J. Y. (2011). Stimulation of ice nucleation by marine diatoms. *Nature Geoscience*, *4*(2), 88–90. <https://doi.org/10.1038/NGEO1037>
- Maahn, M., de Boer, G., Creamean, J. M., Feingold, G., McFarquhar, G. M., Wu, W., & Mei, F. (2017). The observed influence of local anthropogenic pollution on northern Alaskan cloud properties. *Atmospheric Chemistry and Physics*, *17*(23), 14709–14726. <https://doi.org/10.5194/acp-17-14709-2017>
- Matthews, A., & Goldberger, L. A. (2020). *Aircraft-integrated Meteorological Measurement System (AIMMS) instrument handbook (DOE/SC-ARM-TR-260)*. Oak Ridge National Laboratory (ORNL), Atmospheric Radiation Measurement (ARM) Data Center; Pacific Northwest National Laboratory (PNNL). <https://doi.org/10.2172/1725866>
- McCluskey, C. S., Ovadnevaite, J., Rinaldi, M., Atkinson, J., Belosi, F., Ceburnis, D., et al. (2018). Marine and terrestrial organic ice-nucleating particles in Pristine marine to continentally influenced northeast Atlantic Air masses. *Journal of Geophysical Research: Atmospheres*, *123*(11), 6196–6212. <https://doi.org/10.1029/2017JD028033>
- Moallemi, A., Landwehr, S., Robinson, C., Simó, R., Zamanillo, M., Chen, G., et al. (2021). Sources, occurrence and characteristics of fluorescent biological Aerosol particles measured over the Pristine southern ocean. *Journal of Geophysical Research: Atmospheres*, *126*(11), e2021JD034811. <https://doi.org/10.1029/2021JD034811>
- Möhler, O., DeMott, P. J., Vali, G., & Levin, Z. (2007). Microbiology and atmospheric processes: The role of biological particles in cloud physics. *Biogeosciences*, *4*(6), 1059–1071. <https://doi.org/10.5194/bg-4-1059-2007>
- Morrison, D., Crawford, I., Marsden, N., Flynn, M., Read, K., Neves, L., et al. (2020). Quantifying bioaerosol concentrations in dust clouds through online UV-LIF and mass spectrometry measurements at the Cape Verde Atmospheric Observatory. *Atmospheric Chemistry and Physics*, *20*(22), 14473–14490. <https://doi.org/10.5194/acp-20-14473-2020>
- Morrison, H., de Boer, G., Feingold, G., Harrington, J., Shupe, M. D., & Sulia, K. (2012). Resilience of persistent Arctic mixed-phase clouds. *Nature Geoscience*, *5*(1), 11–17. <https://doi.org/10.1038/ngeo1332>
- Moschos, V., Dzepina, K., Bhattu, D., Lamkaddam, H., Casotto, R., Daellenbach, K. R., et al. (2022). Equal abundance of summertime natural and wintertime anthropogenic Arctic organic aerosols. *Nature Geoscience*, *15*(3), 196–202. Article 3. <https://doi.org/10.1038/s41561-021-00891-1>
- Murray, B. J., O'Sullivan, D., Atkinson, J. D., & Webb, M. E. (2012). Ice nucleation by particles immersed in supercooled cloud droplets. *Chemical Society Reviews*, *41*(19), 6519–6554. <https://doi.org/10.1039/c2cs35200a>
- Perring, A. E., Mediavilla, B., Willibanks, G. D., Churnside, J. H., Marchbanks, R., Lamb, K. D., & Gao, R.-S. (2023). Fluorescent Aerosol and meteorological data over the Chukchi and Beaufort Seas, July 2017 (NCEI Accession 0277794) [Dataset]. NOAA. Retrieved from <https://www.ncei.noaa.gov/access/metadata/landing-page/bin/iso?id=gov.noaa.nodc:0277794>
- Perring, A. E., Schwarz, J. P., Baumgardner, D., Hernandez, M. T., Spracklen, D. V., Heald, C. L., et al. (2015). Airborne observations of regional variation in fluorescent aerosol across the United States. *Journal of Geophysical Research-Atmospheres*, *120*(3), 1153–1170. <https://doi.org/10.1002/2014JD022495>
- Pöhlker, C., Huffman, J. A., & Pöschl, U. (2012). Autofluorescence of atmospheric bioaerosols—Fluorescent biomolecules and potential interferences. *Atmospheric Measurement Techniques*, *5*(1), 37–71. <https://doi.org/10.5194/amt-5-37-2012>
- Porter, G. C. E., Adams, M. P., Brooks, I. M., Ickes, L., Karlsson, L., Leck, C., et al. (2022). Highly Active ice-nucleating particles at the summer North Pole. *Journal of Geophysical Research: Atmospheres*, *127*(6), e2021JD036059. <https://doi.org/10.1029/2021JD036059>
- Pöschl, U., Martin, S. T., Sinha, B., Chen, Q., Gunthe, S. S., Huffman, J. A., et al. (2010). Rainforest Aerosols as biogenic nuclei of clouds and precipitation in the Amazon. *Science*, *329*(5998), 1513–1516. <https://doi.org/10.1126/science.1191056>
- Pratt, K. A., DeMott, P. J., French, J. R., Wang, Z., Westphal, D. L., Heymsfield, A. J., et al. (2009). In situ detection of biological particles in cloud ice-crystals. *Nature Geoscience*, *2*(6), 398–401. <https://doi.org/10.1038/ngeo521>
- Prenni, A. J., Harrington, J. Y., Tjernström, M., DeMott, P. J., Avramov, A., Long, C. N., et al. (2007). Can ice-nucleating aerosols affect arctic seasonal climate? *Bulletin of the American Meteorological Society*, *88*(4), 541–550. <https://doi.org/10.1175/BAMS-88-4-541>
- Quinn, P. K., Bates, T. S., Schulz, K., & Shaw, G. E. (2009). Decadal trends in aerosol chemical composition at Barrow, Alaska: 1976–2008. *Atmospheric Chemistry and Physics*, *9*(22), 8883–8888. <https://doi.org/10.5194/acp-9-8883-2009>
- Robinson, E. S., Gao, R.-S., Schwarz, J. P., Fahey, D. W., & Perring, A. E. (2017). Fluorescence calibration method for single-particle aerosol fluorescence instruments. *Atmospheric Measurement Techniques*, *10*(5), 1755–1768. <https://doi.org/10.5194/amt-10-1755-2017>
- Santander, M. V., Mitts, B. A., Pendergraft, M. A., Dinasquet, J., Lee, C., Moore, A. N., et al. (2021). Tandem fluorescence measurements of organic matter and bacteria released in sea spray Aerosols. *Environmental Science & Technology*, *55*(8), 5171–5179. <https://doi.org/10.1021/acs.est.0c05493>
- Savage, N. J., Krentz, C. E., Könemann, T., Han, T. T., Mainelis, G., Pöhlker, C., & Huffman, J. A. (2017). Systematic characterization and fluorescence threshold strategies for the wideband integrated bioaerosol sensor (WIBS) using size-resolved biological and interfering particles. *Atmospheric Measurement Techniques*, *10*(11), 4279–4302. <https://doi.org/10.5194/amt-10-4279-2017>
- Serreze, M. C., & Barry, R. G. (2011). Processes and impacts of Arctic amplification: A research synthesis. *Global and Planetary Change*, *77*(1), 85–96. <https://doi.org/10.1016/j.gloplacha.2011.03.004>
- Schwarz, J. P., Gao, R. S., Fahey, D. W., Thomson, D. S., Watts, L. A., Wilson, J. C., et al. (2006). Single particle measurements of midlatitude black carbon and light-scattering aerosols from the boundary layer to the lower stratosphere. *Journal of Geophysical Research: Atmospheres*, *110*, D16207. <https://doi.org/10.1029/2006JD007076>
- Stein, A. F., Draxler, R. R., Rolph, G. D., Stunder, B. J. B., Cohen, M. D., & Ngan, F. (2015). NOAA's HYSPLIT Atmospheric transport and dispersion modeling system. *Bulletin of the American Meteorological Society*, *96*(12), 2059–2077. <https://doi.org/10.1175/BAMS-D-14-00110.1>



- Tobo, Y., Prenni, A. J., DeMott, P. J., Huffman, J. A., McCluskey, C. S., Tian, G., et al. (2013). Biological aerosol particles as a key determinant of ice nuclei populations in a forest ecosystem. *Journal of Geophysical Research: Atmospheres*, *118*(17), 10100–10110. <https://doi.org/10.1002/jgrd.50801>
- Toprak, E., & Schnaiter, M. (2013). Fluorescent biological aerosol particles measured with the Waveband Integrated Bioaerosol Sensor WIBS-4: Laboratory tests combined with a one year field study. *Atmospheric Chemistry and Physics*, *19*(1), 225–243. <https://doi.org/10.5194/acp-13-225-2013>
- Verlinde, J., Harrington, J. Y., McFarquhar, G. M., Yannuzzi, V. T., Avramov, A., Greenberg, S., et al. (2007). The mixed-phase Arctic cloud experiment. *Bulletin of the American Meteorological Society*, *88*(2), 205–222. <https://doi.org/10.1175/BAMS-88-2-205>
- Wang, X. J., & Key, J. R. (2005). Arctic surface, cloud, and radiation properties based on the AVHRR Polar Pathfinder dataset. Part II: Recent trends. *Journal of Climate*, *18*(14), 2575–2593. <https://doi.org/10.1175/JCLI3439.1>
- Wex, H., Huang, L., Zhang, W., Hung, H., Traversi, R., Becagli, S., et al. (2019). Annual variability of ice-nucleating particle concentrations at different Arctic locations. *Atmospheric Chemistry and Physics*, *19*(7), 5293–5311. <https://doi.org/10.5194/acp-19-5293-2019>
- You, Q., Cai, Z., Pepin, N., Chen, D., Ahrens, B., Jiang, Z., et al. (2021). Warming amplification over the Arctic Pole and Third Pole: Trends, mechanisms and consequences. *Earth-Science Reviews*, *217*, 103625. <https://doi.org/10.1016/j.earscirev.2021.103625>
- Zeppenfeld, S., van Pinxteren, M., Hartmann, M., Bracher, A., Stratmann, F., & Herrmann, H. (2019). Glucose as a potential chemical marker for ice nucleating activity in Arctic seawater and melt Pond samples. *Environmental Science & Technology*, *53*(15), 8747–8756. <https://doi.org/10.1021/acs.est.9b01469>

## Erratum

The originally published version of this article contained some errors in the affiliations. The affiliations for the first author should have been switched. One of the affiliations for the third author, G. Dewey Wilbanks, should have been “Department of Chemistry, Colgate University, Hamilton, NY, USA” rather than “Department of Chemistry, Johns Hopkins University, Baltimore, MD, USA.” The last author’s affiliation should have been “Earth Systems Research Laboratory, National Oceanic and Atmospheric Administration, Boulder, CO, USA” rather than “Now at Department of Earth and Environmental Engineering, Columbia University, New York, NY, USA.” The affiliations have been corrected, and this may be considered the authoritative version of record.